Anthraquinonedisulfonate Adsorption, Electron-Transfer Kinetics, and Capacitance on Ordered Graphite Electrodes: The Important Role of Surface Defects

Mark T. McDermott, Kristin Kneten, and Richard L. McCreery*

Department of Chemistry, The Ohio State University, 120 W. 18th Avenue, Columbus, Ohio 43210
(Received: October 3, 1991; In Final Form: December 12, 1991)

The adsorption of anthraquinone-2,6-disulfonate, disodium salt (AQDS), was found to be well behaved at glassy carbon (GC) and highly oriented pyrolytic graphite (HOPG) electrodes. On laser-activated GC, the surface excess obeys a Langmuirian isotherm in the concentration range of 5×10^{-8} to 1×10^{-5} M with a saturation coverage of 228 pmol/cm^2. AQDS at untreated HOPG electrodes was studied more extensively. Adsorption at basal plane HOPG was discovered to occur solely on edge plane defects. Defects on basal plane HOPG can be created adventitiously in the cleaving process or can be controlled by laser irradiation at varying power densities. The amount of AQDS adsorbed correlates with laser power density. Surface excess on HOPG also obeys a Langmuir isotherm with the saturation coverage depending on the defect density. On conventionally cleaved HOPG surfaces, the amount of AQDS adsorption correlates with other electrochemical parameters, the magnitudes of which are known to depend on edge plane density. These parameters are the heterogeneous electron-transfer rate constant of the ferri/ferrocyanide redox couple and differential capacitance. A new low differential capacitance of less than 1.0 μF/cm^2 has also been observed on near-perfect basal plane HOPG. The unusual ferrocyanide voltammograms observed on low-defect HOPG are consistent with a potential-dependent transfer coefficient.

Introduction

The widespread use of carbon electrodes in energy conversion, electrosynthesis, and electroanalysis has stimulated a wide variety of research on the relationship between carbon structure and electrochemical behavior.[1,2] While it is recognized that carbon microstructure, surface oxides, and adsorbed films will affect electrode kinetics, capacitance, etc., these structural variables are often difficult to control. Several reports from our group[3-6] and others[7-12] have identified the importance of basal and edge plane graphite regions to electrochemical behavior, and noted that the distribution of edge and basal sites on a carbon surface varies greatly for different carbon substrates and surface preparations. The difficult problem of relating surface structure to electrochemical behavior is significantly simplified by examining a nearly ideal surface, namely, the basal plane of highly ordered pyrolytic graphite (HOPG). The basal plane has a known distribution of carbon atoms and provides a single-crystal analogue of more disordered carbon materials. The purpose of this paper is to characterize the basal plane surface of nearly perfect HOPG and to examine its electrochemical properties.

HOPG is a highly anisotropic material, exhibiting quite different properties on its basal and edge planes. Physical properties of HOPG, such as resistivity, thermal conductivity, thermal expansion, and Young's modulus, display anisotropy with sometimes large differences between the in-plane (a-axis) and out-of-plane (c-axis) directions.[2] Raman spectroscopy of HOPG also depends on this anisotropy, with the ratio of 1360-cm^{-1}/1582-cm^{-1} band intensities correlating with graphitic edge plane density.[4,5] Our group and others have reported anisotropy in the double-layer capacitance (C°)[3,6,7-10] and heterogeneous electron-transfer rate constant (k°)[3,5,6,11,12] for some benchmark redox systems, with both C° and k° being higher for edge vs basal plane HOPG. The density of edge plane sites on HOPG can be increased greatly by illumination with energetic laser pulses, apparently by thermomechanical shock induced by rapid thermal expansion.[3,4,6] We showed that k° of $Fe(CN)_6^{3-/4-}$ correlated with C° for laser-irradiated HOPG, implying that both are related to laser-generated edge plane.[6] Adventitious edge plane defects resulting from the cleaving of HOPG are known to be sites for other phenomena. Eklund et al.[13] have reported intercalation of HSO_4^- through the basal plane of HOPG. They concluded that the intercalant enters through grain boundaries and/or accidental defects on the surface. Damage caused by electrochemical oxidation of basal plane HOPG has been shown by Raman spectroscopy,[4,5] scanning electron microscopy (SEM),[4] and scanning tunneling microscopy (STM) to initiate on edge defects.[14] Chang and Bard observed that defects on freshly exposed basal plane occurred at a density of 0.1-13 μm^{-2} for various samples of HOPG.[15] Snyder et al.[16] used STM to observe polymers preferentially nucleating at step sites on basal plane HOPG. Recently, we have shown that adventitious defects on HOPG electrodes affect electrochemical parameters in ways similar to those created intentionally. A more defective surface as observed by STM exhibits a higher k° for ferri/ferrocyanide and a larger C°.[3] Accidental edge plane defects cause considerable statistical variation in the measurement of these two parameters. The results also indicate strong adsorption of anthraquinone-2,6-disulfonate (AQDS) to edge plane sites and weak adsorption to basal plane. All of these phenomena indicated the importance of edge plane defects to HOPG behavior.

The pronounced anisotropy of HOPG leads to several serious problems when examining electrochemical variables on carbon electrodes. First, capacitance, k°, and adsorption often vary greatly with the proportions of edge and basal plane on the exposed surface, as has been noted previously in some detail.[3,6,17] Thus GC exhibits faster kinetics than HOPG basal plane because of its higher edge plane density. Second, supposedly ordered HOPG

* Author to whom correspondence should be addressed.

(1) Kinoshita, K. *Carbon: Electrochemical and Physicochemical Properties*; Wiley: New York, 1988.
(2) McCreery, R. L. In *Electroanalytical Chemistry*; Bard, A., Ed.; Dekker: New York, 1991; Vol. 17.
(3) Robinson, R. R.; Sternitzke, K.; McDermott, M. T.; McCreery, R. L. *J. Electrochem. Soc.* **1991**, *138*, 2454.
(4) Bowling R.; Packard, R.; McCreery, R. L. *J. Am. Chem. Soc.* **1989**, *111*, 1217.
(5) Bowling R.; Packard, R. T.; McCreery, R. L. *Langmuir* **1989**, *5*, 683.
(6) Rice, R. J.; McCreery, R. L. *Anal. Chem.* **1989**, *61*, 1637.
(7) Morcos, I.; Yeager, E. *Electrochim. Acta* **1970**, *15*, 953.
(8) Randin, J. P.; Yeager, E. *J. Electroanal. Chem.* **1972**, *36*, 257.
(9) Randin, J. P.; Yeager, E. *J. Electrochem. Soc.* **1971**, *118*, 711.
(10) Randin, J. P.; Yeager, E. *J. Electroanal. Chem.* **1975**, *58*, 313.
(11) Wightman, R. M.; Paik E. C.; Borman, S.; Dayton, M. A. *Anal. Chem.* **1978**, *50*, 1410.
(12) Wightman, R. M.; Deakin, M. R.; Kovach, P. M.; Kuhr, P. M.; Stutts, K. J. *J. Electrochem. Soc.* **1984**, *131*, 1578.
(13) Eklund, P. C.; Oik, C. H.; Holler, F. J.; Spolar, J. G.; Arakawa, E. T. *J. Mater Res.* **1986**, *1* (2), 361.
(14) Gewirth, A. A.; Bard, A. J. *J. Phys. Chem.* **1988**, *92*, 5563.
(15) Chang, H.; Bard, A. J. *J. Am. Chem. Soc.* **1991**, *113*, 5588.
(16) Snyder, S. R.; White, H. S.; Lopez, S.; Abruna, H. D. *J. Am. Chem. Soc.* **1990**, *112*, 1333.
(17) Rice, R. J.; Pontikos, N. M.; McCreery, R. L. *J. Am. Chem. Soc.* **1990**, *112*, 4618.

0022-3654/92/2096-3124$03.00/0

basal plane surfaces exhibit quite variable electrochemical behavior, depending on the presence of adventitious (or intentional) defects.[3,6] For example, $k°$ may vary significantly with repeated cleavage of HOPG, due to variations in surface defects from cleave to cleave.[3] Third, any measurement of inherent basal plane properties is likely to be contaminated by the effects of edge plane defects, and this problem is severe when the anisotropy is large. For example, when $k°$ is 0.1 cm/s on the edge and 10^{-7} cm/s on basal plane (approximate values for $Fe(CN)_6^{3-/4-}$),[6] even 0.1% of edge plane defects on a basal surface will yield observed "basal" rate constants about 1000 times too large. Thus any attempt to study electrochemical properties of the ordered HOPG basal plane is likely to be frustrated by the effects of a low level of defects. The long-range goal of the effort presented here is observation of basal plane properties which are uncontaminated by the properties of edge plane defects and thus representative of an ordered carbon surface.

The electrochemical behavior of mono- and disulfonated anthraquinones has been the topic of several investigations, and the adsorption of these sulfonated anthraquinones on metals and carbon has been noted previously.[18-20] Soriaga and Hubbard showed that anthraquinone-2,6-disulfonate (AQDS) adsorbs at platinum electrodes in a close-packed, flat orientation.[18] More recently, He et al.[19] demonstrated that AQDS exhibited a well-behaved, reversible adsorption voltammogram on mercury at bulk concentrations below 10^{-5} M. Brown and Anson examined the adsorption of anthraquinone-2-monosulfonate (AQMS) at pyrolytic graphite (PG) electrodes.[20,21]

The approach used here starts with a more detailed examination of AQDS adsorption on edge plane defects. Once AQDS adsorption is established as a useful quantitative marker of defect density, it can be correlated with other defect-dependent electrochemical variables, including capacitance and $k°$ for $Fe(CN)_6^{3-/4-}$. Such correlations are useful not only for establishing the existence of a nearly defect free basal plane surface, but also for determining the electrochemical properties of an ordered graphite electrode surface.

Experimental Section

All solutions were prepared with distilled water purified with a Nanopure water purification system and degassed with argon. Potassium ferrocyanide was used as received from Mallinckrodt Inc., and solutions of 1 mM $K_4Fe(CN)_6$ in 1 M KCl were prepared daily. Disodium AQDS was obtained from Aldrich and recrystallized from water after filtering through activated charcoal.[19] Solutions of AQDS in 0.1 M $HClO_4$ degrade after 2–3 days and were prepared accordingly. All experiments were conducted at 23 ± 2 °C.

For experiments on GC, a Bioanalytical Systems GC-20 electrode embedded in Kel-F was utilized. The GC electrode was conventionally polished before laser activation and GC experiments were performed in a Teflon cell as previously described.[17] HOPG was either purchased from Union Carbide (Parma, OH) or was a gift from Arthur Moore of Union Carbide. HOPG samples are graded by Union Carbide according to the line width of the X-ray diffraction peak, with greater line width corresponding to smaller microcrystallite size along the a-axis. Grades are as follows: ZYA, ≤0.4°; ZYB, 0.8 ± 0.2°; ZYH, 3.5 ± 1.5°. HOPG surfaces were prepared either by peeling with adhesive tape or by cleaving with a razor blade. Surfaces of "pure" basal plane (very low defects) were obtained by cleaving a thick piece (ca. >5 mm along the c-axis) of HOPG with a razor blade. Since cleaving with adhesive tape imposed curvature on the graphite being removed and to a lesser extent on the sample, the resulting mechanical strain appeared to create defects. Cleaving with the razor blade did not cause curvature and led to low-defect surfaces. Laser activation of HOPG was performed in situ with solution present in a cell described previously.[6] All other electrochemical experiments were carried out in an inverted drop cell. The HOPC was peeled or cleaved and fastened to a conductive metal plate with powdered graphite/nujol paste to assure good electrical contact. A drop of solution was then placed on the fresh basal plane surface. A platinum wire auxiliary electrode and a capillary salt bridge containing a Ag/AgCl (3 M NaCl) reference electrode were lowered into the drop to complete the cell. This type of "cell" eliminates factors such as damage to the surface from an O-ring and impurities from the Teflon cell. Because the solution was placed on the electrode within 10–15 s of peeling or cleaving, surface contamination was minimized. Edge plane HOPG electrodes were imbedded in Torr-Seal (Varian) as previously reported.[6]

Adsorption of AQDS was quantified by measuring the baseline-corrected area under the voltammetric reduction wave as described by Brown and Anson.[21] The diffusion wave for AQDS was too small to interfere with measurements of the adsorption peak and was displaced far away on the potential axis.[3] Adsorption was monitored with time until a constant value was observed, with longer times being required for lower AQDS concentrations. AQDS data are reported here as Γ_{obs}, the observed adsorption in picomoles per square centimeter, and Γ_{sat}, the saturated adsorption at high bulk concentration of AQDS, denoted C_{AQDS}. The observed $k°$ for $Fe(CN)_6^{4-/3-}$ ($D = 6.3 \times 10^{-6}$ cm^2/sec) is reported as $k°_{obs}$ and was calculated from ΔE_p via the method of Nicholson in most cases.[22] Where noted, simulations based on a potential-dependent transfer coefficient according to the approach of Corrigan and Evans[23] were used to determine $k°_{obs}$. Observed differential capacitance, reported as $C°_{obs}$, was measured with a 20-mV peak-to-peak, 100-Hz triangle wave centered at 0.0 V vs Ag/AgCl using the method developed by Gileadi et al.[24,25] and used by us previously.[3,6,17] All electrode areas used for calculations were measured by chronoamperometry of 1 mM $Fe(CN)_6^{4-}$ on a 5-s time scale. Cyclic voltammetry and laser activation with a Nd:YAG laser operating at 1064 nm were performed as described previously.[3-6,17]

Results

The voltammetry of 10^{-5} M AQDS at a GC electrode laser irradiated with three 25 MW/cm^2 Nd:YAG pulses is shown in Figure 1A. Laser activation of GC at this power density serves to clean the surface of impurities and polishing debris.[17,26] At this low concentration of AQDS, the peak diffusion current should be approximately 0.01 mA/cm^2 and is negligible on the scale of Figure 1A. The peak current in Figure 1A is directly proportional to scan rate for the wave centered at −0.1 V vs Ag/AgCl. Peak width at half-maximum (pwhm) for this wave is 55 mV, and the cathodic/anodic peak separation is 12 mV at 1 V/s and 5 mV at 100 mV/s. For a reversible adsorption wave, the theoretical pwhm is $90.6/n$, where $n = 2$ for AQDS, and the peak separation is zero.[27,28] The data indicate that at low concentrations AQDS is a quasi-reversible surface-bound redox center at GC electrodes.

An adsorption isotherm was obtained for bulk concentrations of AQDS from 5×10^{-8} to 2×10^{-6} M. Curve A in Figure 2 is the surface excess vs bulk concentration plot for AQDS at a GC electrode. This curve is characteristic of a Langmuir isotherm.[27,28] Peak shape, potential, and half-width do not change with concentration. These results imply minimal interaction between surface-bound molecules at low bulk concentrations and provide strong evidence for an adsorbed species adhering to a Langmuir isotherm. It is clear that AQDS is a well-behaved surface-bound species on laser-activated GC at low bulk concentrations.

(18) Soriaga, M. P.; Hubbard, A. T. *J. Am. Chem. Soc.* **1982**, *104*, 2735.
(19) He, P.; Crooks, R. M.; Faulkner, L. R. *J. Phys. Chem.* **1990**, *94*, 1135.
(20) Anson, F. C.; Epstein, B. *J. Electrochem. Soc.* **1968**, 1155.
(21) Brown, A. P.; Anson, F. C. *Anal. Chem.* **1977**, *49*, 1589.
(22) Nicholson, R. S. *Anal. Chem.* **1965**, *37*, 1351.
(23) Corrigan, D. A.; Evans, D. H. *J. Electroanal. Chem.* **1980**, *106*, 287.
(24) Gileadi, E.; Tshernikovski, N. *Electrochim. Acta* **1971**, *16*, 579.
(25) Gileadi, E.; Tshernikovski, N.; Babai, M. *J. Electrochem. Soc.* **1972**, *119*, 1018.
(26) Pontikos, N. M.; McCreery, R. L. *J. Electroanal. Chem.*, in press.
(27) Laviron, E. *J. Electroanal. Chem.* **1982**, *12*, 53.
(28) Bard, A. J.; Faulkner, L. R. *Electrochemical Methods*; Wiley: New York, 1980.

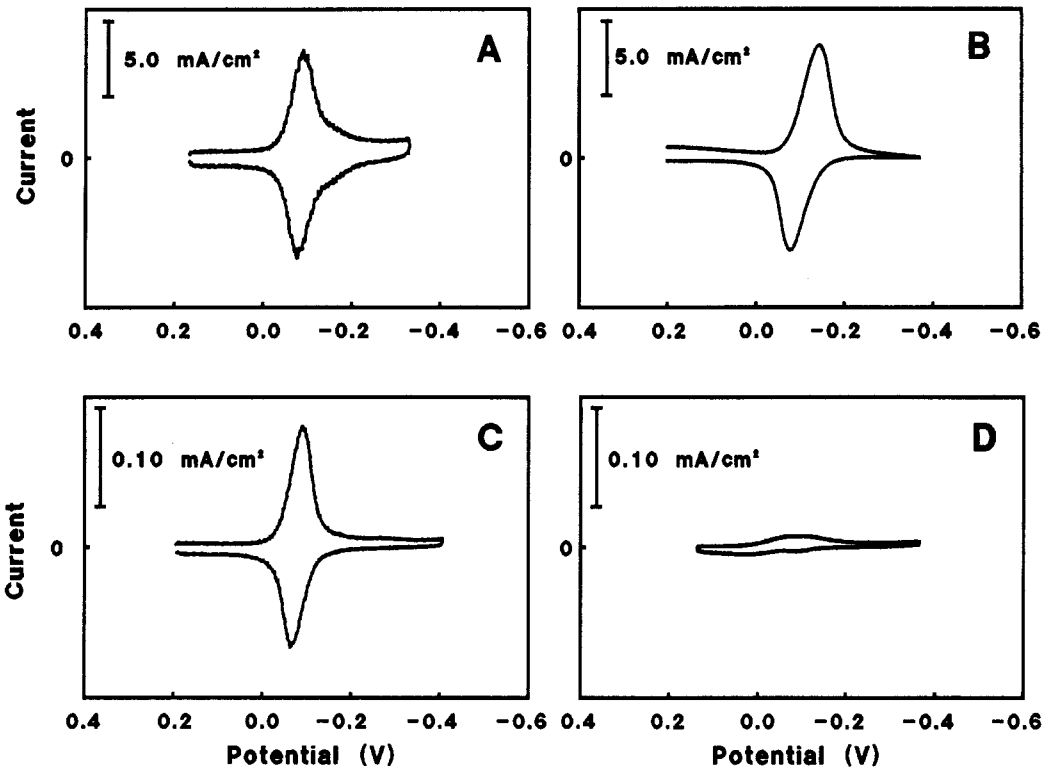

Figure 1. Cyclic voltammetry of 10^{-5} M AQDS at (A) GC electrode activated with three 25 MW/cm² laser pulses; (B) edge plane HOPG; (C) basal plane HOPG with visible defects; (D) basal plane HOPG with few defects. Scan rate = 1 V/s. Potentials are vs Ag/AgCl.

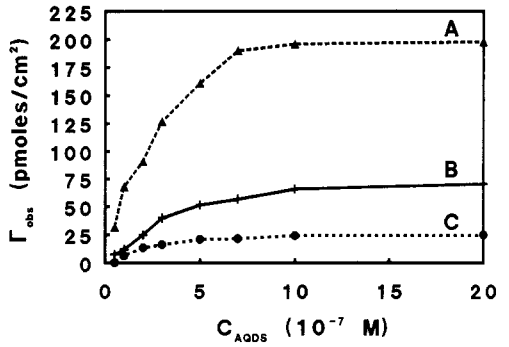

Figure 2. Amount of AQDS adsorbed vs bulk concentration on (A) GC, laser activated at 25 MW/cm²; (B) basal plane HOPG, laser activated at 70 MW/cm²; (C) basal plane HOPG, laser activated at 50 MW/cm². The lines simply connect the points and do not assume any theoretical equation. Adsorption time was at least 20 min.

Parts B–D of Figure 1 were obtained under the same conditions as part A, but with various HOPG surfaces. Voltammogram B is HOPG edge plane (embedded in Torr-Seal), and voltammograms C and D were obtained on two different basal plane surfaces with the inverted drop "cell". Except for current magnitude, the voltammograms in Figure 1 exhibit comparable pwhm and ΔE_p, with the only exception being the slightly larger ΔE_p for HOPG edge plane (possibly due to Torr-Seal contamination). Inspection of the current scales of Figure 1 reveals the effect of edge plane density on the quantity of AQDS adsorbed, since the peak current for an adsorbed species is proportional to the quantity adsorbed. Electrodes rich in edge plane such as GC and edge plane HOPG (Figure 1A,B) yield approximately 50 times greater current than basal plane HOPG with visible defects created in the cleaving process (Figure 1C). The voltammogram of Figure 1D occurred on an HOPG surface which had no visible defects. The absence of a voltammetric wave for AQDS on basal plane indicates either that AQDS does not adsorb on basal plane or that any adsorbed AQDS does not undergo electron transfer to basal plane. In either case, Γ_{obs} increases with greater edge plane density.

Since the voltammograms of Figure 1C,D were obtained on HOPG basal surfaces prepared in the same manner, it is clear that the defect density varies significantly from surface to surface. This conclusion is not surprising, but it does prevent preparation of surfaces with reproducible defect density by conventional cleaving. In order to examine AQDS adsorption on HOPG basal plane more quantitatively, we used laser irradiation to generate reproducibly defective surfaces. In earlier reports, we showed that Nd:YAG laser pulses damaged the HOPG surface at power densities of 45 MW/cm² and higher.[3,6] Furthermore, both capacitance and $k°_{obs}$ for $Fe(CN)_6^{3-/4-}$ increased with increasing laser power, implying a higher density of edge sites. Accordingly, AQDS adsorption was examined on laser-treated HOPG in order to study a more reproducibly damaged surface, with the results shown in Table I. All voltammograms of AQDS on laser-activated HOPG indicated ideal adsorption and were qualitatively very similar to those of Figure 1C. Isotherms for the 50 and 70 MW/cm² cases are shown in Figure 2. While the shapes are comparable to that observed for GC, saturation coverage is lower.

TABLE I: Observed Adsorption of AQDS and $k°$ of $Fe(CN)_6^{3-/4-}$ on Laser-Irradiated Basal Plane HOPG

power density, MW/cm²	Γ_{obs}, pmol/cm²	$k°_{obs}(Fe(CN)_6^{3-/4-})$, cm/s
50	35 (σ = 1.2)	0.042 (σ = 0.0090)
60	44 (σ = 1.1)	0.065 (σ = 0.0092)
70	70 (σ = 1.4)	0.093 (σ = 0.010)
80	82 (σ = 1.7)	0.096 (σ = 0.0046)
90	96 (σ = 2.8)	0.110 (σ = 0.0057)
100	140 (σ = 14)	0.130 (σ = 0.0058)

[a] σ is standard deviation, N = 3 in all cases.

The equation of a Langmuir isotherm can be linearized in the form

$$\frac{C_{AQDS}}{\Gamma_{obs}} = \frac{1}{\Gamma_{sat} b_{AQDS}} + \frac{C_{AQDS}}{\Gamma_{sat}} \quad (1)$$

where Γ_{obs} is the surface excess of AQDS, Γ_{sat} is the saturation surface excess, b_{AQDS} is the adsorption coefficient of AQDS the on the particular surface, and C_{AQDS} is the bulk concentration. Figure 3 shows the linearized data of Figure 2, and Table II lists the data obtained from the isotherm of AQDS at several electrodes. In the case of HOPG, the saturation coverage is dependent

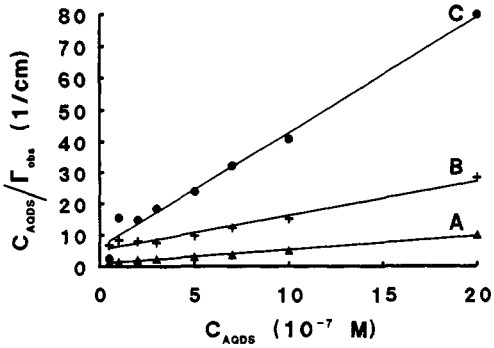

Figure 3. Linearized data from Figure 2. A, B, and C correspond to the same surfaces as in Figure 2. The lines are the least-squares fit to the data, with $r \geq 0.99$ for all lines.

TABLE II: Adsorption Isotherm Results for AQDS[a]

surface	Γ_{obs}, Γ_{sat}, pmol/cm^2	b_{AQDS}, cm^3/mol	ref
GC, 25 MW/cm^2	228	6×10^9	this work
HOPG, 70 MW/cm^2	92	2×10^9	this work
HOPG, 50 MW/cm^2	28	4×10^9	this work
Hg	94	7×10^9	19
Pt	127[b]		18
PG	140[b]		20

[a] Determined from linearized Langmuir equation as described in text. [b] Not determined from a complete isotherm.

on laser-induced damage. For comparison, saturation coverages for AQDS on other surfaces are also given in Table II. The increase in Γ_{obs} for the series HOPG (basal) < HOPG (laser) < PG < GC is consistent with the increase in disorder and edge plane density for these materials.[2] Although studied in less detail, anthraquinonemonosulfonate and 1,5-AQDS behave quite similarly to AQDS with small differences in Γ due to varying molecular size. The differences in the magnitude of AQDS adsorption on platinum vs mercury have been attributed to a very substantial dissimilarity in surface bonding.[19] On the basis of the approach of Soriaga and Hubbard, the theoretical saturation coverage for AQDS on a flat surface is 132 pmol/cm^2.[18]

Table I also lists the observed k°_{obs} for $Fe(CN)_6^{3-/4-}$ on laser-treated surfaces, in order to compare with Γ_{obs}. As noted previously, k°_{obs} increases with increasing laser power density above the 45 MW/cm^2 threshold.[6] The k°_{obs} values observed here follow the same trend as those reported previously,[6] but are consistently higher, probably due to greater cleanliness accompanying irradiation in solution rather than air. In order to make a similar correlation of Γ_{obs} and k°_{obs} on untreated basal plane, it was necessary to measure Γ_{obs} and k°_{obs} on the *same* surface. Thus a voltammogram of $Fe(CN)_6^{3-/4-}$ was acquired on a freshly cleaved surface with the inverted drop "cell", and then the solution was replaced and Γ_{obs} was determined. In addition, C°_{obs} was determined in the $Fe(CN)_6^{3-/4-}$ or AQDS solution. In this way, C°_{obs}, k°_{obs}, and Γ_{obs} were measured on a surface with a given defect density, effectively controlling for variations in defects from surface to surface. The results for 42 basal plane surfaces are listed in Table III, in order of increasing Γ_{obs}. With the exception of the laser-treated surfaces, the Γ, k°_{obs}, and C°_{obs} values listed for a given electrode were determined on the same surface by the inverted-drop approach. Parameters determined on laser-treated surfaces were reproducible from surface to surface, and entries in Table III are averages of three surfaces. Notice that k°_{obs} and C°_{obs} increase monotonically with Γ_{obs}, implying that all three observables are controlled by similar surface effects.

Representative voltammograms obtained with several surfaces exhibiting varying ΔE_p are shown in Figure 4. For $\Delta E_p < 200$ mV, the voltammograms have shapes consistent with conventional Nicholson and Shain theory.[22,29] However, when ΔE_p exceeds 200 mV, distortions from classical behavior are evident, with serious disagreement with theory at ΔE_p of above 300 mV. The scan rate dependence of this distortion is shown in Figure 5 for

TABLE III: Surface Coverage of AQDS, Kinetic Parameters of $Fe(CN)_6^{4-/3-}$, and Differential Capacitance for Basal Plane HOPG

grade/prep.[a]	Γ_{obs}, pmol/cm^2	ΔE_p,[b] mV	k°_{obs}, cm/s	C°_{obs}, μF/cm^2
U/C	<1.0	1500	8.0×10^{-7}[c]	0.6[d]
U/C	<1.0			0.8[e]
U/C	<1.0			0.9[e]
U/C	<1.0			1.0[e]
U/C	1.0	1020	8.0×10^{-6}[c]	1.4[d]
U/C	1.1	770	6.1×10^{-5}[c]	1.5[d]
U/C	2.1	970	9.2×10^{-6}[c]	1.7[d]
U/C	3.5	740	7.5×10^{-5}[c]	1.5[d]
U/C	8.0			1.8[e]
A/C	11	470	2.8×10^{-4}[c]	
A/C	14	300	0.0014[c]	1.2[d]
A/C	14	130	0.0085	
B/C	24	203	0.0032	2.9[d]
H/C	25	168	0.0049	
B/C	25	165	0.0057	
A/C	26	103	0.015	
A/C	26	95	0.019	
U/C	30	122	0.010	3.1[d]
H/C	34	144	0.0068	3.6[d]
U/L(50)	35	78	0.042	3.4[d]
H/C	38	97	0.018	
H/C	40	122	0.010	
H/C	41	120	0.011	
H/C	41	93	0.020	
U/L(60)	44	84 (5)	0.065	
H/C	45	114	0.012	
H/C	52	100	0.015	
H/C	55	80	0.036	4.2[d]
H/C	56			4.7[e]
H/C	58	106	0.014	5.2[d]
H/C	62			5.3[e]
H/C	64	87	0.025	5.8[d]
H/C	65	83	0.030	
A/C	67	78	0.041	5.8[d]
U/C	69	92	0.021	6.5[d]
U/L(70)	70	79 (5)	0.093	
H/C	73	114	0.012	6.7[d]
U/L(70)	75			8.2[e]
U/L(80)	82	77 (5)	0.096	
H/C	85	85	0.030	
U/L(90)	96	81 (10)	0.110	
U/L(100)	142	76 (10)	0.130	

[a] Grade: U = ungraded; A = ZYA; B = ZYB; H = ZYH. Preparation: C = cleaved; L = laser activated; power density in MW/cm^2 listed in parentheses. [b] ν = 1.0 V/s unless indicated in parentheses. [c] k°_{obs} calculated by simulation with potential-dependent α; all others from ΔE_p by method of Nicholson. [d] C°_{obs} measured in 1.0 M KCl. [e] C°_{obs} measured in 0.1 M $HClO_4$.

TABLE IV: Voltammetric Results for Single HOPG Basal Surface with Low Defect Density

ν, V/s	ΔE_p, mV	k°_{NS},[a] cm/s	k°_{sim},[b] cm/s	α_0[b]	dα/dE[b]
10	1238	4.6×10^{-7}	9.6×10^{-6}	0.50	0.25
5	1132	8.1×10^{-7}	1.1×10^{-5}	0.50	0.27
1	940	2.4×10^{-6}	1.6×10^{-5}	0.49	0.27
0.5	896	2.5×10^{-6}	1.6×10^{-5}	0.50	0.28
0.1	808	2.6×10^{-6}	1.1×10^{-5}	0.50	0.28
0.05	755	3.2×10^{-6}	1.1×10^{-5}	0.51	0.29

[a] Calculated by method of Nicholson,[22] using $D = 6.3 \times 10^{-6}$ cm^2/s. [b] Best fit of experimental and simulated voltammograms assuming a potential-dependent α.

ΔE_p = 940 mV (at 1 V/s), and voltammetric results for various scan rates are listed in Table IV. Although there is no doubt that the large ΔE_p indicates slow electron-transfer kinetics, the voltammograms on low-defect surfaces clearly do not exhibit classical behavior.

Discussion

The variations in k°_{obs}, C°_{obs}, and Γ_{obs} for different HOPG basal plane surfaces establish the importance of surface defects in determining electrochemical parameters. AQDS is a useful marker

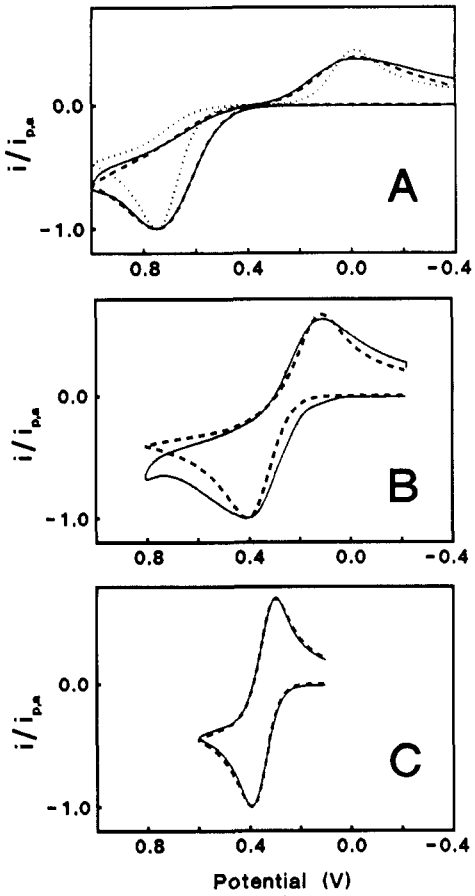

Figure 4. Voltammograms of $Fe(CN)_6^{3-/4-}$ (1 M KCl) on three HOPG basal plane surfaces with different defect density. Solid lines are experimental in all cases. (A) Dashed line, simulated for $k^\circ_{obs} = 6.1 \times 10^{-5}$ cm/s, $\alpha_0 = 0.51$, $d\alpha/dE = 0.30$ V^{-1}; dotted line, simulated for $k^\circ_{obs} = 1.2 \times 10^{-5}$ cm/s, $\alpha = 0.51$, $d\alpha/dE = 0.0$. (B) Dashed line, simulated for $k^\circ_{obs} = 1.4 \times 10^{-3}$ cm s^{-1}, $\alpha_0 = 0.50$, $d\alpha/dE = 0.30$ V^{-1}. (C) Dashed line simulated for $k^\circ_{obs} = 0.018$ cm s^{-1}, $\alpha_0 = 0.50$, $d\alpha/dE = 0.30$. Simulation for $d\alpha/dE = 0.0$ is identical to dashed line. Scan rate = 1.0 V/s in all cases. Potentials are vs Ag/AgCl.

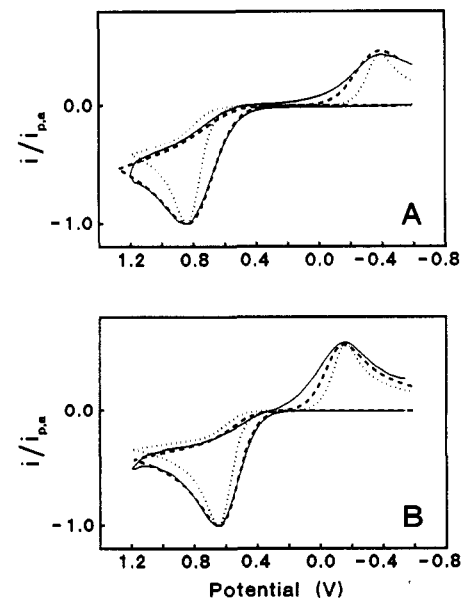

Figure 5. Voltammograms of $Fe(CN)_6^{3-/4-}$ (1 M KCl) on cleaved HOPG at two scan rates on a low defect surface. Solid line is experimental in both cases. (A) 10 V/s; dashed line is simulated for $k^\circ_{obs} = 9.6 \times 10^{-6}$ cm/s, $\alpha_0 = 0.50$, $d\alpha/dE = 0.25$ V^{-1}; dotted line is same, except $k^\circ_{obs} = 4.6 \times 10^{-7}$ cm/s and $d\alpha/dE = 0$. (B) 0.1 V/s, dashed line is simulated for $k^\circ_{obs} = 1.1 \times 10^{-5}$ cm/s, $\alpha_0 = 0.51$, $d\alpha/dE = 0.29$ V^{-1}. Dotted line is simulation for $k^\circ_{obs} = 2.6 \times 10^{-6}$ cm/s, $\alpha_0 = 0.51$, $d\alpha/dE = 0.0$.

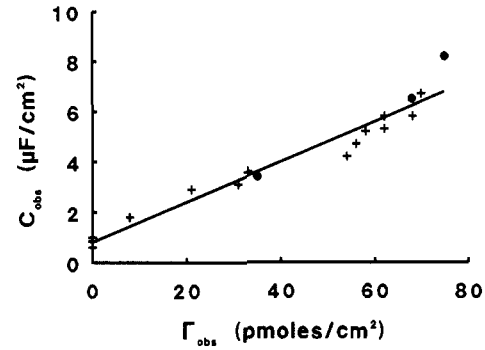

Figure 6. Plot of differential capacitance, C°_{obs}, vs Γ_{obs}. Points are laser surfaces, pluses are cleaved. Line is least-squares fit to all points.

for defect density, with Γ_{obs} ranging from near zero on low-defect basal plane HOPG up to roughly monolayer coverage on GC. Since C°_{obs}, k°_{obs}, and Γ_{obs} are all much higher on edge vs basal plane, they should track the edge plane density as indicated by Γ_{obs}. In addition, the observed k°_{obs} should correlate with Γ_{obs}, since both observables depend on edge plane density. In the simplest case, one might propose that the electrode area covered by adsorbed AQDS equals the defect area. However, this proposal is probably oversimplified due to the unkown microscopic details of AQDS adsorption on defects of various size and shape. For now, it is sufficient to conclude that increased Γ_{AQDS} indicates a greater number of edge plane defects. A variety of defects have been reported for HOPG basal plane, including step edges, missing atoms, atomic scale ridges, and fissures.[3,15,29] As stated earlier, Chang and Bard noted a wide variation in defect density observed by STM, ranging from 0.1 to 13 defects/μm^2.[15] In some cases, these defects have been misinterpreted in STM images as adsorbed molecules, such as DNA.[30] In light of the correlation between Γ_{obs} and purposely induced defects (via laser activation or the use of GC), it is very likely that AQDS adsorption occurs on the STM-observable defects on HOPG. Given the strong adsorption of AQDS on Pt, Hg, and pyrolytic graphite reported by others,[18,20] it is not surprising that saturation coverage is achieved on GC and laser-damaged HOPG at bulk concentrations below 10^{-5} M. The 228 pmol/cm^2 [18] saturation coverage for GC is higher than that predicted on the basis of molecular size for flat adsorption (132 pmol/cm^2). Either the AQDS is not lying flat, or the GC surface has a roughnesss factor of $228/132 \cong 1.7$. Of course, the roughness will depend on surface preparation, but values for GC ranging from 1.4 to 2.5 have been reported for polished GC following laser activation.[17] While the flat orientation of adsorbed AQDS is not established by the current results, it is the most likely, and the implied roughness factor is within the range expected. In the case of basal plane HOPG, Γ_{AQDS} approaches and exceeds a theoretical monolayer with laser activation.[17,26] As deduced from STM,[3] this indicates both defect formation and roughening by the laser. However, the 10^3–10^5-fold increase in k°_{obs} accompanying laser activation cannot be due soley to roughening, and the major factor in laser activation of HOPG is defect formation.

In order to consider the effect of surface defects more quantitatively, we should first examine the result that Γ_{obs}, C°_{obs} and k°_{obs} for $Fe(CN)_6^{3-/4-}$ all correlate for a series of untreated basal plane surfaces (Table III) and laser-treated basal plane (Table I and ref 6). As noted earlier Γ_{obs}, C°_{obs}, and k°_{obs} all track defect density, and should therefore trace each other. Figure 6 is a plot of C°_{obs} vs Γ_{obs} for both untreated and laser-activated surfaces. Figure 7 shows k°_{obs} vs Γ_{obs}, plotted in log–log format to cover the wide range. Recall that each point on Figures 6 and 7 represents two measurements performed on the *same* surface, largely correcting for unavoidable variation in defect density from surface to surface. The first conclusion from these results is simple but important: the lowest values of C°_{obs}, Γ_{obs}, and k°_{obs} most accurately reflect true basal plane properties. Since even a small

(29) Nicholson, R. S.; Shain, I. *Anal. Chem.* **1964**, *36*, 706.
(30) Clemmer, C. R.; Beebe, T. P. *Science* **1991**, *251*, 640.

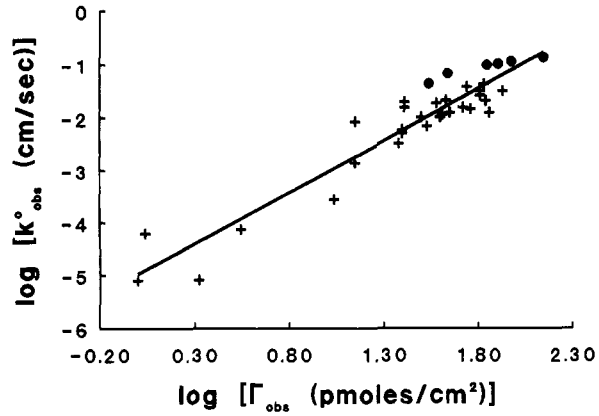

Figure 7. Logarithmic plot of observed adsorption of AQDS, Γ_{obs}, on basal HOPG vs observed heterogeneous electron rate constant, k°_{obs}, of 1 mM $Fe(CN)_6^{4-/3-}$ in 1 M KCl. Pluses indicate cleaved surfaces, points indicate laser treatment. Line is least-squares fit for all points.

defect density can have a large effect on electrochemical observables (particularly k°_{obs}), the true basal plane behavior will be masked by defect behavior unless the defect density is low. In the case of capacitance, C°_{obs} was always below 1.0 $\mu F/cm^2$ when Γ_{obs} was below its detection limit, with the lowest observed value being 0.6 $\mu F/cm^2$. Since the slope of C°_{obs} vs Γ_{obs} is not very steep, the C°_{obs} on a genuinely perfect HOPG surface is not likely to be much lower than 0.6 $\mu F/cm^2$. The best estimate of C°_{obs} for perfect basal plane capacitance is the intercept of the least-squares line in Figure 6, 0.81 $\mu F/cm^2$, with an upper limit of 1.0 $\mu F/cm^2$. This result is lower than that reported by Yeager (3.0 $\mu F/cm^{-2}$),[8-10] due to lower defect density in the present case or to the difference in the method of measurement. The implications of this low capacitance are noted below.

It is not so easy to deduce the true basal plane k° for $Fe(CN)_6^{3-/4-}$, given the much stronger dependence of k°_{obs} on defect density. Variations in Γ_{obs} near the detection limit (< 1.0 pmol/cm²) correspond to large variations in ΔE_p (1020–1500 mV), so it is hard to determine k°_{obs} for a zero-defect surface. Stated differently, even a few ppm of defects (which would be below the detection limit for Γ_{obs}) can significantly increase k°_{obs}, so only an upper limit for k°_{obs} on perfect basal plane may be determined. We conclude that perfect basal plane exhibits a ΔE_p of >1500 mV at 1.0 V/s, leading to a k°_{obs} of $< 10^{-6}$ cm/s.

The second observation available from Figures 6 and 7 involves the functional dependence of electrochemical variables on defect density. On the basis of the STM-determined defect density of 0.1–13 μm^{-2}, defects are rarely more than 1 μm apart, and are themselves much less than 1 μm in size.[3,15] At scan rates in the range of 0.1–10 V/s, the defects will behave as a random array of microelectrodes spaced much closer than $(Dt)^{1/2}$. This situation has been considered by Amatore et al.[31] and Armstrong et al.[32,33] for the case of small active sites. In the case of basal plane HOPG, the active sites are not the oxides proposed by Armstrong et al., the unblocked surface assumed by Amatore et al., or the active redox sites proposed by Kuwana et al.[34] for GC, but rather are edge plane defects exhibiting much higher k°_{obs} than the surrounding undamaged basal plane. When the sites are close to each other compared to $(Dt)^{1/2}$, the surface will behave like an ordinary planar microelectrode with a smaller k°_{obs} than that of the active sites. Stated differently, if diffusional cross talk is rapid between active and less active surface regions, the observed k°_{obs} is an average of rate constants for active and less active areas, weighted by surface coverage.[2,31] Even the smallest k° observed here for basal plane HOPG may be due to very small defects spaced closer than $(Dt)^{1/2}$. It is useful to consider a weighted average of basal and edge regions for determining electrochemical observables as a first approximation. Such as assumption leads to eq 2 for capacitance,[6] where f_e is the fractional area of edge

$$C^\circ_{obs} = C^\circ_{basal}(1 - f_e) + C^\circ_{edge} f_e \quad (2)$$

plane present on the surface. For Γ_{obs}, we can assume that Γ on basal plane is zero, so

$$\Gamma_{obs} = \Gamma_{sat} f_e \quad (3)$$

Substituting for f_e in eq 2 yields

$$C^\circ_{obs} = C^\circ_{basal}\left(1 - \frac{\Gamma_{obs}}{\Gamma_{sat}}\right) + C^\circ_{edge}\left(\frac{\Gamma_{obs}}{\Gamma_{edge}}\right) \quad (4)$$

or

$$C^\circ_{obs} = C^\circ_{basal} + \frac{\Gamma_{obs}}{\Gamma_{sat}}(C^\circ_{edge} - C^\circ_{basal}) \quad (5)$$

Equation 4 predicts linearity for the plot of Figure 6, with an intercept equal to C°_{basal}. As noted earlier, the least-squares line for all points of Figure 6 yields an intercept of $C^\circ_{basal} = 0.81$ $\mu F/cm^2$.

For the case of k°_{obs}, the analogous linear approximation is inadequate to explain Figure 7. For laser-activated surfaces, covering a range of Γ_{obs} from 35 to 140 pmol/cm² (Table I), the slope of the log k°_{obs} vs log Γ_{obs} has a slope of 1.2, implying proportionality. However, the slope of the line for all points in Figure 7 is 1.9, a value inconsistent with proportionality of k°_{obs} and Γ_{obs}. These observations are consistent with a linear dependence of C°_{obs}, k°_{obs}, and Γ_{obs} on the fractional coverage of edge plane defects on the basal surface for laser-activated surfaces, but the linear model fails for the near-perfect basal plane.

Additional insight into the kinetic behavior of HOPG surfaces is provided by the deviation of voltammogram shape on low-defect surfaces from that predicted by conventional Nicholson and Shain theory. As shown in Figure 4, peak widths and relative heights differ significantly from conventional theory as ΔE_p increases. This distortion could originate in several different aspects of the experiment. First, it could be caused by some inherent basal plane property which becomes important only at low defect densities, when edge plane contributions to kinetics are minimized. For example, Gerisher[35] and Randin and Yeager[7-10] concluded that basal plane HOPG has a low density of states and a low capacitance, with both reaching a minimum at about −0.2 V vs saturated calomel electrode. Either effect could lead to slow kinetics, particularly near the potential of zero charge (PZC). Second, the distortion could be caused by a potential-dependent transfer coefficient (α) which becomes important as ΔE_p increases.[23,36] For large ΔE_p, the oxidation and reduction are occurring at quite different potentials, and a nonconstant α is likely. Third, the distortion may be caused by some characteristic of the defects acting as microelectrodes. For the small and infrequent defects present on near-perfect surfaces, the double layer may be nonplanar, and unusual double-layer effects may occur, particularly near the PZC.[36]

The distortion occurs for any voltammogram with $\Delta E_p \geq 200$ mV, for which k°_{obs} is < 0.003 cm/s. This k°_{obs} is much greater than the upper limit for k°_{basal} (10^{-6} cm/s), so a voltammogram with ΔE_p = 200–400 mV has negligible contribution from basal plane. Thus the distortion is unlikely to be caused by unusal basal plane properties, since distortion occurs when the rate is still controlled largely by defects. The possibility of a potential-dependent α was tested by simulating several voltammograms with an α which depended linearly on potential, according to the method of Corrigan and Evans.[23] Figure 4A shows a simulated curve for $\alpha_0 = 0.50$ and $d\alpha/dE = 0.25$ V^{-1}, as well as the conventional simulation ($d\alpha/dE = 0$). For small ΔE_p (<200 mV), inclusion

(31) Amatore, J. M.; Saveant, J. M.; Tessier, D. J. *J. Electroanal. Chem.* **1983**, *147*, 39.
(32) Armstrong, F. A.; Bond, A. M.; Hill, A. O.; Psalti, I. S. M.; Zoski, C. G. *J. Phys. Chem.* **1989**, *93*, 6485.
(33) Armstrong, F. A.; Bond, A. M.; Hill, A. O.; Oliver, N.; Psalti, I. S. M. *J. Am. Chem. Soc.* **1989**, *111*, 9185.
(34) Hu, I. F.; Kuwana, T. *Anal. Chem.* **1986**, *58*, 3235.
(35) Gerisher, H. *J. Phys. Chem.* **1985**, *89*, 4249.
(36) Norton, J. D.; White, H. S.; Feldberg, S. W. *J. Phys. Chem.* **1990**, *94*, 6772.

of $d\alpha/dE$ made little difference to wave shape (Figure 4C), but it did significantly affect curves for $\Delta E_p > 500$ mV. Figure 5 shows experimental and simulation cyclic voltammograms for two scan rates on a low-defect surface, demonstrating a marked effect of nonconstant α on the wave shape. The fits of theory and experiment shown in Figures 4A and 5 and in Table IV are quite good, supporting the conclusion that a potential-dependent α is important when ΔE_p is large. Theory and experiment agree less well for intermediate ΔE_p (Figure 4B), perhaps because the surface is quite defective ($f_e \sim 1$-3%) and irregular. Although these observations do not prove that a potential-dependent α is the sole origin of the distortion from conventional shape, they do indicate that the observations are consistent with a nonconstant α.

Regardless of the details of the shape of the cyclic voltammograms on low-defect surfaces, there is no doubt that the observed kinetics are very slow for $Fe(CN)_6^{3-/4-}$ on the basal plane. We have reported similarly slow kinetics and basal plane for dopamine[4] and solution-phase AQDS.[3] Sufficient data are not yet available to ascertain the generality of slow basal plane kinetics, and until such data are available, it would be risky to speculate an underlying phenomeon causing slow kinetics. The results on AQDS adsorption, capacitance, and $Fe(CN)_6^{3-/4-}$ kinetics reported here establish a means to reduce or eliminate contamination of basal plane behavior by edge plane defects. We are currently studying a wide range of redox systems on low-defect basal plane surfaces, in order to determine the phenomena controlling the electrochemical behavior of the basal plane. The results will be reported separately.

In summary, k°_{obs}, C°_{obs}, and Γ_{obs} for AQDS are controlled largely by defects on basal plane HOPG, and all three observables vary greatly for different surfaces. Although perfect basal plane has a C°_{obs} below 1.0 $\mu F/cm^2$, a k°_{obs} for $Fe(CN)_6^{3-/4-}$ below 10^{-6} cm/s, and negligible AQDS adsorption, observed values are usually higher due to adventitious or intentional defects. Since all three phenomena depend on defect density, they correlate with each other provided they are measured on the same plane surface. The voltammetry of $Fe(CN)_6^{3-/4-}$ on partly defective basal plane is consistent with a potential-dependent transfer coefficient, which is a major factor when ΔE_p exceeds about 500 mV at 1 V/s. Finally, the reason for the very slow kinetics of $Fe(CN)_6^{3-/4-}$ on basal plane is not yet clear, but is currently being addressed by studying a variety of redox systems on low-defect basal plane surfaces.

Acknowledgment. This work was supported by the Air Force Office of Scientific Research. We acknowledge Dr. Arthur Moore at Union Carbide for the generous gift of HOPG and Dennis Evans for the simulation software. We also thank Christie Allred for many useful discussions and software for electrochemical experiments.

Computation of the Electrostatic Interaction Energy between a Protein and a Charged Surface

Byung Jun Yoon† and Abraham M. Lenhoff*

Department of Chemical Engineering, University of Delaware, Newark, Delaware 19716
(Received: November 14, 1991)

Protein–surface interactions play a central part in many situations both in vivo and ex vivo, but it is not yet possible to predict the extent of interaction quantitatively as a function of protein structure and surface and solution properties. A method for doing so is presented for systems dominated by electrostatic interactions, based on a continuum model of the electrostatic potential in and around a protein molecule near a charged surface in an electrolyte solution. The governing equations are solved by a boundary element approach which uses the method of images to treat the presence of an infinite planar charged surface exactly without any truncation. The potential distribution is used to obtain the protein–surface interaction energy; the boundary element approach allows this to be done rigorously, without approximating the self-energy contribution. The method is applied to determining the electrostatic interaction between a positively charged ribonuclease A molecule and a negatively charged surface at various orientations and separations. The strongest electrostatic attraction is found for ribonuclease A with its active site facing the surface, while in certain orientations the interaction can be repulsive.

Introduction

Interactions between protein molecules and solid–liquid interfaces are important in many applications,[1,2] such as chromatographic separation of proteins, the design of biocompatible materials for medical uses, and food processing. In addition, protein–surface interactions are important in vivo, e.g., in the approach of proteins to membrane surfaces. The protein–surface interaction is extremely complex, involving the interplay of many physical and chemical factors. In principle, the evolution of configurational changes of the protein–surface system can be examined theoretically using the equations of motion for each protein atom, and results based on molecular mechanics and dynamics computations are emerging.[3] However, because of the structural complexities of the protein molecule, solution, and solid surface, analysis at the atomic level remains very difficult.

A less extreme degree of reductionism, applicable under conditions where the protein structure does not change appreciably due to interaction with the surface, is to treat the protein molecule as a rigid particle. Here information furnished in terms of the interaction potential energy between the molecule and the surface can be used to determine equilibrium states or to follow the dynamics by integration of the equation of motion for the molecule. The interactions are entirely electromagnetic in nature, but they are usually analyzed using continuum models[4] in which the overall interaction is decomposed into parts, e.g., van der Waals inter-

* To whom correspondence should be addressed.
† Present address: Department of Chemical Engineering, POSTECH, P.O. Box 125, Pohang 790-600, Korea.

(1) MacRitchie, F. *Adv. Protein Chem.* **1978**, *32*, 283-326.
(2) Andrade, J. D.; Hlady, V. *Adv. Polym. Sci.* **1986**, *79*, 1-63.
(3) Lim, K.; Herron, J. N. In *Biomedical Applications of Polyethylene Glycol Chemistry*; Harris, J. M., Ed.; Plenum, New York, in press. Lu, D. R.; Lee, S. J.; Park, K. *J. Biomater. Sci. Polym. Ed.* **1991**, *3*, 127-147.
(4) Israelachvili, J. N. *Intermolecular and Surface Forces*; Academic Press: New York, 1985.

0022-3654/92/2096-3130$03.00/0